scientific reports

Check for updates

OPEN

A novel hexagonal PtPS monolayer for high anisotropic carrier mobility and potential for photocatalytic water splitting with pronounced optical absorption

Chunying Pu, Pan Zhang, Linxuan Chen, Xindong Pan & Dawei Zhou✉

Low symmetry two-dimensional noble-metal phosphochalcogenides MPX (M = Pd, Pt; X = S, Se, Te) with an unusual orthorhombic structure and pentagons attracted tremendous attention in recent years for their potential applications in optoelectronic, photocatalysts, thermoelectric devices. Motivated by the attractive properties and potential applications of MPX materials, we identified a novel stable hexagonal structure of PtPS monolayer with the space group $P\bar{3}m1$ using particle swarm optimization algorithms in conjunction with first-principles calculations. We not only evaluate its stability by calculations of the phonon dispersion, molecular dynamic simulation and elastic constants, but also investigate its structural, electronic, carrier mobility, optical and photocatalyst properties. The PtPS monolayer is a semiconductor with an indirect band gap of 1.23 eV (using the PBE functional) and 1.84 eV (using the HSE06 functional). More importantly, the PtPS monolayer demonstrates high electron mobility along the y direction and pronounced anisotropy, which can effectively enhance the separation of the photogenerated electrons and holes, thereby reducing recombination and improve photocatalytic activity. The photocatalytic calculations reveal that the band-edge alignments of the PtPS monolayer perfectly span the redox potential of water, providing a robust driving force for the convention of H_2O into H_2 and O_2, making it effective in both acidic and neutral environments. Furthermore, Optical calculations demonstrate that PtPS monolayer exhibit outstanding light absorption in both visible and ultraviolet spectrum ranges, with the absorption coefficient reaching up to the order of 10^5 cm^{-1} and a high solar-to-hydrogen efficiency (16.0%). Our research suggests that the excellent properties of hexagonal PtPS monolayer can provide a guidance for experimental studies and the development of new functional layered materials based on PtPS.

Keywords First principles, Structure prediction, PtPS semiconductor, Photocatalysis

Since graphene was successfully exfoliated[1], two dimensional (2D) materials have garnered extensive attention due to their unique physical and chemical properties[2]. It is well known that graphene is considered a promising material for electronic device due to its excellent carrier mobility[3,4]. However, the absence of a band gap in graphene significantly limits its practical applications[5]. Therefore, the alternative 2D semiconductor materials with a suitable band gap have been explored and investigated by theoretical predictions and experimental realization in the past decades. These 2D semiconductor materials including phosphorene[6], transition metal dichalcogenides (TMDC)[7,8], carbon nitrides[9–11], monochalcogenides[12,13], etc., have been studied for their potential application in optoelectronics, electronics, and energy storage. Among them, TMDC always attracted much attention and have potential in the next generation of electronic devices owing to their changeable electronic structure and transport properties. Particularly, two dimensional noble-metal dichalcogenide MX_2 (M = Pd, Pt; X = S, Se, Te)[14–23] have drawn more attention and research on their applications in spintronic, optoelectronic, sensors, photocatalysts, and thermoelectric devices in recent few years. Different from the well-known 2 H- or 1 T TMDC materials, noble-metal dichalcogenide MX_2 displays a distinctive orthorhombic structure, characterized by unique building blocks such as pentagons and MX_4 planar squares. These materials

College of Physics and Electronic Engineering, Nanyang Normal University, Nanyang 473061, China. ✉email: zhoudawei@nynu.edu.cn

have been effectively synthesized using various techniques, including mechanical exfoliation, molecular beam epitaxy (MBE) growth, chemical vapor transport, or sulfurization methods. The typical penta-PdX_2 not only display the layer-dependent band gaps[24], but also exhibit excellent thermoelectric performance[25,26] and field effect transistor performance[27,28].

The orthogonal phase of noble-metal dichalcogenide PdX_2 with pentagonal structure spurred numerous theoretical and experimental study on the chemical substitution for X atom replaced by the same family or P element to explore exceptional physical and chemical properties. Ryu et al.[29] studied the structure, electronic transport, and thermoelectric properties of the $PdSe_{2-x}S_x$ and found that the S substitution can effectively change the electronic structure of $PdSe_2$. Using First principles, Xiao et al.[30] discovered that the penta-PdSSe possesses desirable band gaps, outstanding light absorption properties and exceptionally high carrier mobilities. These characteristics make the PdSSe monolayer a highly promising candidate for use in optoelectronic, photocatalysis, and nanoelectronics. Recently, layered PdPS and PdPSe featuring orthogonal lattice structures[31] can be exfoliated from their bulk forms with a cleavage energy of 0.6 J/m^2 in theoretically, of which 2D PdPSe with a puckered structure was follow experimentally exfoliated by Li et al.[32]. Subsequently, penta- PdPSe and PdPS were also synthesized via chemical vapor transport and exhibits the thickness-dependence electrical properties, which can be as field effect transistor[33,34]. The penta-PdPSe were observed to have a high strong anisotropic electrical conductivity and a high photo response[35]. It's optical properties, electronic structure simulation reveal that the penta-PdPSe is a promising material for photocatalytic water splitting. Huang et al.[36] studied that noble metal phosphochalcogenides PtPX(X = S, Se, Te) with pentagonal shape have the moderate carrier mobility and high ZT values at 800 K and can be used in thermoelectric and electrical transport devices.

Given the intriguing properties and promising potential applications of the penta-MPX materials[37,38], there is a significant interest in investigating their novel ground-state structures and predicting their physical and chemical properties. In this work, we aim to discover a new low energy PtPS structure by employing a global structure search approach integrated with first-principles calculations. One stable hexagonal PtPS monolayer has been predicted with P-P bond two 1 T-type PtPS monolayer. In particular, PtPS monolayer exhibits a suitable band gap, anisotropic high carrier mobilities, excellent absorption capability. Notably, the band edge positions of the PtPS monolayer meet the criteria for photocatalytic water splitting under both acidic and neutral conditions with a high solar-to-hydrogen efficiency, highlighting its potential as an ideal material for water-splitting applications.

Computational method

The search for the PtPS monolayer structure was performed using a particle-swarm optimization algorithm, which was executed within the CALYPSO program[39–41] in conjunction with first principles calculations. Simulation cells containing 1, 2, 3, and 4 formula units were considered for PtPS monolayer. To guarantee convergence, both the population size and the number of generations were set at 40. In this study, geometry relaxation, total energy calculations, electronic structure analysis, and optical property evaluations were performed using the VASP software[42], which is based on density functional theory (DFT). The electron-ion interactions were described using projected-augmented-wave(PAW) potentials[43,44], while the exchange-correlation energy was approximated using the Generalized Gradient Approximation (GGA) with Perdew-Burke-Ernzerhof (PBE) functional[45]. To ensure convergence, a plane-wave cut-off energy of 520 eV was used for all calculations. During the structure relaxations, k point spacing of the reciprocal space was set to 0.03 A^{-1}, which is $10 \times 10 \times 1$ k point mesh in PtPS monolayer. A vacuum spacing of 27.0 Å was introduced in the z-direction to minimize the effects of weak van der Waals forces between adjacent layers. The self-consistent field calculations were performed with convergence criteria set to an energy tolerance of 1×10^{-6} eV/atom and a maximum atomic force of 0.001 eV/atom. To obtain an accurate band gap and optical absorption spectra, the Heyd-Scuseria-Ernzerhof (HSE06)[46,47] method was employed for calculating the band structures and optical properties. The dynamic stability of the PtPS monolayer was assessed by computing the phonon spectra for a $4 \times 4 \times 1$ supercell using the finite displacement approach within the Phonopy package[48]. Ab *initio* molecular dynamics simulations (AIMD) were carried out using the NVT canonical criterion for a $3 \times 3 \times 1$ supercell structure at a temperature of 300 K with a time step of 1 fs for running 10 ps.

The carrier mobility is estimated based on the deformation potential approximation and expressed as[49,50]

$$\mu_{2D} = \frac{e\hbar^3 C_{2d}}{k_B T |m^*|^2 (E_l)^2} \tag{1}$$

where $\hbar$ represents the Planck constant, k_B is the Boltzmann constant, m^* denotes effective mass along the both transport direction, T is the temperature, set to 300 K. The deformation potential constant, E_l, corresponds to the valence band maximum (for holes) and the conduction band minimum (for electrons) in the transport direction. The in-plane elastic modulus, C_{2D}, is derived from the relationship $2(E - E_0)/S_0 = C_{2d} \times (\Delta l/l_0)^2$, where E is the total energy, E_0 is the equilibrium energy, and S_0 is the equilibrium lattice area of the 2D structure.

Results and discussion

Structure and stability

By employing the structure search method within the CALYPSO program, two lower-energy penta-like PtPS structures were firstly identified: one structure with the space group $P2/c$ (No. 13), referred to as the α phase, and another structure with the space group $Pmc21$ (No. 26), termed the β phase[51,52]. These structures were reproduced after a sixteen-generation search using 4 formula units. Additionally, a novel lower-energy structure with 2 formula units was discovered and is illustrated in Fig. 1. The structure of the PtPS monolayer belongs to

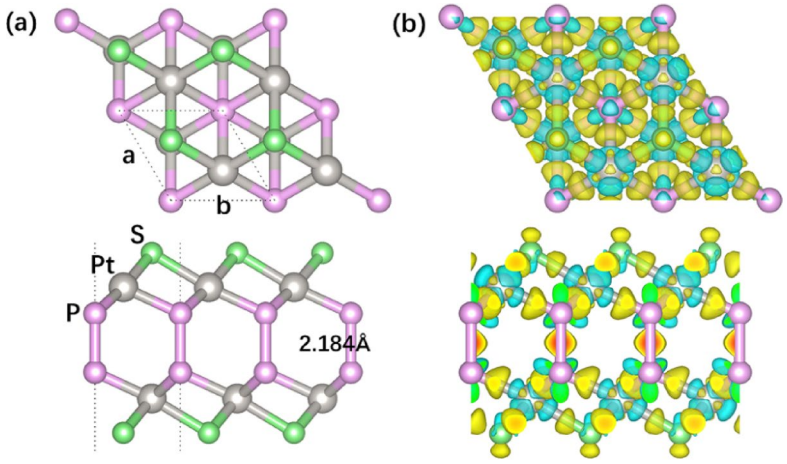

Fig. 1. Top and side views of the (**a**) PtPS monolayer structure with the dotted line representing the unit cell and (**b**) charge density difference of the PtPS monolayer. Pt, S, and P atoms are depicted as gray, green, and pink spheres, respectively. The gold regions represent areas of charge accumulation, while the cyan regions indicate charge depletion. The isosurface value is set 0.012e $Å^{-3}$.

the space group $P\bar{3}m1$ with hexagonal primitive unit cell, consisting of 2 Pt, 2 P and 2 S atoms. The P-P bonds shown in Fig. 1a connect the two sublayers similar to 1 T-MoS_2 that make the properties of hexagonal PtPS monolayer different from those of penta-like structures. The calculated lattice constant of a or b is 3.683 Å, and the optimized Pt–P, Pt-S, and P–P bond distances are 2.344, 2.482, and 2.184 Å, respectively.

To further analyze the chemical bonding, the charge density difference of the PtPS monolayer was computed, as illustrated in Fig. 1b. This difference is defined as the total electron density of the PtPS system minus the electron densities of isolated Pt, P, and S atoms at their corresponding positions. It is notable that the charges are predominantly concentrated in the middle of the P-P bond, forming a nonpolar covalent bond between the nearest two P atoms. Whereas for the Pt-S and Pt-P bond, the transfer charges are shifted toward S and P atoms, suggesting the presence of polar covalent bonds between Pt-S and Pt-P. According to Bader charge analysis, each Pt atom transfers a net electronic charge of 0.3 and 0.8 |e| to S and P atoms, respectively.

To assess the stability of crystal binding, the cohesive energy per atom was determined using the following formula

$$E_{\mathrm{coh}} = \frac{E_{\mathrm{tot}}(\mathrm{PtPS}) - \sum n_{\mathrm{i}} E_{\mathrm{i}}}{\sum n_{\mathrm{i}}} \tag{2}$$

Where $E_{\mathrm{tot}}(\mathrm{PtPS})$represents the total energy of PtPS, n_{i} is the number of Pt, P, and S atoms in the unit cell, and E_{i} is the energies of single Pt, P, and S atoms. The cohesive energy of hexagonal PtPS monolayer is −5.65 eV/atom. The negative values indicate that predicted hexagonal PtPS is energetically more stable than the isolated atoms. Although the cohesive energy value of hexagonal PtPS is larger than the values of pentagonal α phase (−5.74 eV/atom) and β phase (−5.72 eV/atom) (this work), this small energy difference implies that the hexagonal PtPS monolayer could potentially be synthesized by optimizing experimental conditions, such as temperature, pressure, and the surrounding gas.

The phonon dispersion spectrum of the PtPS monolayer was calculated to assess dynamic stability. Figure 2a displays the calculated phonon curve, which exhibits entirely positive frequencies throughout the Brillouin zone, indicating that the PtPS monolayer is dynamically stable and can be controlled to experimental acquisition. We also conducted molecular dynamics simulations to evaluate the stability of PtPS monolayer at a temperature of 300 K. We provide snapshots of the atomic structure during the dynamic simulation process at 10 ps with a time step of 1 fs, as illustrated in Fig. 2b. The PtPS supercells exhibited no significant atomic rearrangement or bond breaking. This indicates that the PtPS monolayer is thermodynamically stable at room temperature. Additionally, we further examine the mechanical stability of PtPS monolayer by calculating its linear elastic constants. Due to hexagonal symmetry, three independent elastic constants are calculated to be C_{11} = 180.86, C_{12} = 66.12, and C_{66} = 57.37 Nm^{-1}, which satisfied the elastic stability criteria[53]: $C_{11}C_{22} - C_{12}^2 > 0$, $C_{66} > 0$ and $C_{11} > |C_{12}|$, indicating the PtPS monolayer is mechanical stable. The Young's modulus is also calculated to be 156.69 Nm^{-1} by $Y = (C_{11}^2 - C_{12}^2)/C_{11}$, much larger than that of MoS_2 monolayer (129 N·m−1)[54], confirming the strong bonding in hexagonal PtPS monolayer.

Electronic structure and carrier mobility

To comprehend the electronic characteristics of the hexagonal PtPS monolayer, the electronic band structure and projected density of states were first computed and shown in Fig. 3a. Since first-principles calculations with the PBE functional tend to underestimate material band gaps, we calculated the band gaps of the PtPS monolayer using the HSE functionals for a more accurate assessment. The PtPS monolayer is an indirect semiconductor

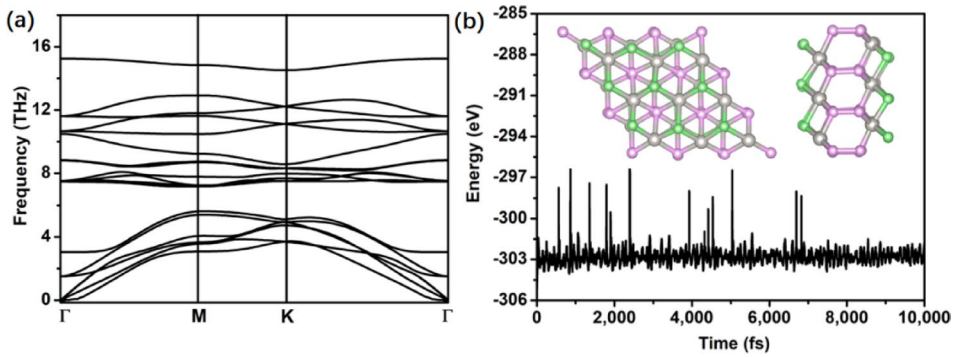

Fig. 2. (**a**) Phonon spectrum of 2D PtPS monolayer; (**b**) Energy as a function of AIMD steps at 300 K. The inset shows the final configuration from the molecular dynamics simulation at 300 K.

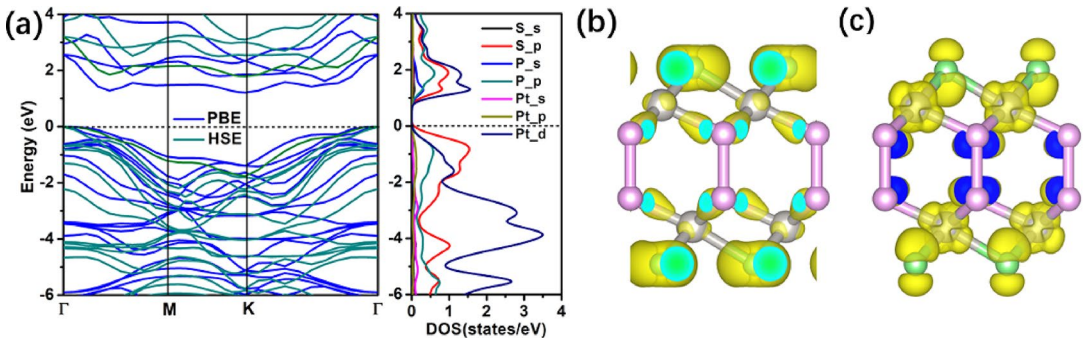

Fig. 3. (**a**) Energy band structure plots and projected density of states for the PtPS monolayer. The real-space charge distribution of the (**b**) VBM and (**c**) CBM of the PtPS monolayer. The iso-surface value is 0.005 e bohr^{-3}.

and its band gap is 1.23 eV and 1.84 eV with the PBE and HSE06 functional, respectively. As indicated by the band structures, the PtPS monolayer has a valence band maximum (VBM) that situated at the Γ point (0, 0, 0), whereas the conduction band minimum (CBM) is positioned at the high symmetry K point (−1/3, 2/3, 0). The projected density of states indicated that the VBM of PtPS monolayer is mainly occupied by S-p orbitals and the CBM is mainly derived from the Pt-d and S-p orbitals. This observation aligns with the real-space charge distribution of the VBM (Fig. 3b) and CBM (Fig. 3c).

To prevent the electron-hole recombination, carrier mobility is a crucial indication in the design of photocatalytic materials. The carrier mobilities are strongly affected by the carrier effective mass, the deformation potential constant near the VBM and CBM, and the in-plane elastic modulus. We computed the effective masses of electrons and holes, which are obtained by second polynomial fitting to the CBM (electron) and VBM (hole) along x and y directions of the orthogonal supercell as shown inset of Fig. 4a, which is built to investigate the carrier conduction behavior intuitively. From the band structure (Fig. 3a), it is evident that the valence band is relatively flat, suggesting a large effective mass for holes. As listed in Table 1, the effective mass for holes is 2.154 m_e (2.135 m_e) along x(y) directions, nearly the two times that of the electron effective mass (1.073 m_e and 1.065 m_e along x and y directions, respectively).

The deformation potential constant E_l is another critical parameter, determined by linearly fitting the conduction band minimum (CBM) and valence band maximum (VBM) using the vacuum energy level as a reference, both of which vary with applied strain. The variation of the band edges with strain in the x and y directions is shown in Fig. 4b. The deformation potential is equal to the slope of the fitted lines. Table 1 shows that the E_l of VBM and CBM along x direction are bigger than the E_l in the y directions, suggesting that the band edge along x direction are more susceptible to strain. Figure 4a illustrates the variation in total energy as a function of applied strain along the x and y directions. We derived the in-plane stiffness $C_{2\,d}$ by fitting the energy-strain curves. As shown in Fig. 4a, the two curves are nearly identical, and the difference in $C_{2\,d}$ along the two directions is minimal, as detailed in Table 1 (171.17 and 172.08 N/m along the x and y directions, respectively).

On the basis of the obtained values E_l, $C_{2\,d}$, m^*, and the carrier mobility at room temperature using Eq. (1) are calculated to be listed in Table 1. There are significant differences between the mobilities of electrons (36.69/5049.35 cm^{2}V^{-1}s^{-1}) and holes (6.09/220.42 cm^{2}V^{-1}s^{-1}) along x/y directions, exhibiting pronounced anisotropy. The substantial anisotropy in carrier mobilities primarily arises from the distinct deformation potentials of the valence band maximum (VBM) and conduction band minimum (CBM) along the x and y directions. Along the same direction, the ratio of electron/hole mobility are 6.02 (22.90) along the x(y) direction,

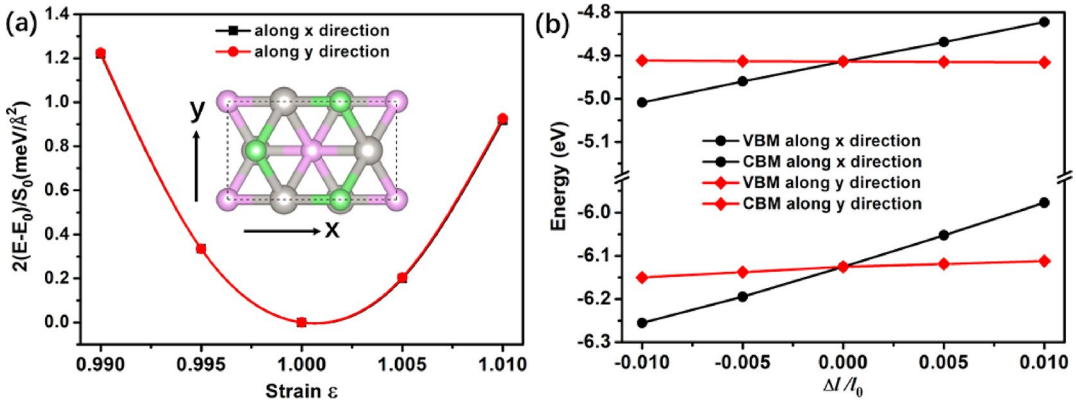

Fig. 4. (**a**) The total energy shift as a function of lattice deformation along x and y direction in the orthogonal supercell atomic structure (inset) of PtPS monolayer. (**b**) Shifts of the valence band maximum and conduction band minimum under uniaxial strain along x and y direction.

Structure	Carrier type	E_l (eV)	C_{2d} ($N\,m^{-1}$)	$m^*(m_e)$	μ ($cm^2V^{-1}s^{-1}$)
$P\bar{3}m1$	e(*x*)	9.29	171.17	1.073	36.69
	h(*x*)	11.36	171.17	2.154	6.09
	e(*y*)	−0.8	172.08	1.065	5049.35
	h(*y*)	1.91	172.08	2.135	220.42

Table 1. Calculated deformation potential parameters (E_l), 2D elastic modulus (C_{2d}), effective mass (m^*), and mobility for electron (e) and hole (h) along the x and y directions at 300 K for the PtPS monolayer.

which indicates that the transport behaviors of electrons and holes are markedly different in both directions. The anisotropic behavior of charge carriers facilitates the efficient separation of photogenerated electrons and holes, suppressing the probability of recombination, which is advantageous for improving the efficiency of photocatalytic water splitting.

Photocatalytic and optical properties

In general, two-dimensional semiconductors with band gaps ranging from 1.5 to 3.0 eV are highly promising candidates for photocatalytic applications. The band gap value of$P\bar{3}m1$PtPS monolayer meets the minimum energy requirement of 1.23 eV for driving photocatalytic water splitting[55]. Another crucial criterion is that the conduction band minimum should be positioned higher than the hydrogen reduction potential (H^+/H_2), while the valence band maximum should be lower than the water oxidation potential (H_2O/O_2). In the case of water, the standard reduction potential of H^+/H_2 and oxidation potential of H_2O/O_2 based on the redox potential of water can be evaluated and is given by the following Eqs. 6[56,57]

$$\mathrm{E}^{\mathrm{reduction}}(\mathrm{H}^+/\mathrm{H}_2) = -4.44 + \mathrm{pH} \times 0.059\mathrm{eV} \tag{3}$$

$$\mathrm{E}^{\mathrm{oxidation}}(\mathrm{H}_2\mathrm{O}/\mathrm{O}_2) = -5.67 + \mathrm{pH} \times 0.059\mathrm{eV} \tag{4}$$

Typically, the reduction potential of H^+/H_2 and oxidation potential of H_2O/O_2 are estimated at pH = 0 for acidic conditions and pH = 7 for neutral conditions. The redox potential varies depending on the specific reaction involved.

The alignments of the CBM and VBM was calculated using the highly accurate HSE functional, with the results presented in Fig. 5. The VBM lies below the oxygen evolution potential (H_2O/O_2, −5.67 eV) and the CBM is above the hydrogen evolution potential (H^+/H_2, −4.44 eV). This band alignment satisfies the thermodynamic criteria for photocatalytic water splitting under acidic conditions. It is worth mentioning that photocatalytic water splitting typically takes place in a neutral environment. Obviously, the VBM is below the oxygen evolution potential (H_2O/O_2, −5.257 eV) and the CBM exceeds hydrogen evolution potential (H^+/H_2, −4.027 eV) at neutral environment, still fulfilling the requirement of the photocatalyst environment. Overall, the requirements for the band gap and band edge positions of an ideal photocatalyst are high. For example, the relatively high position of VBM and the low position of the CBM in certain 2D materials, such as black phosphorus (BP) with the higher VBM, restricted their applicability in photocatalytic water splitting. Additionally, the direct band gap of BP is not conductive to reducing the carrier recombination rate[58]. Furthermore, the band edge positions of the material are well suited for photocatalytic water splitting under a range of pH conditions. It is challenging for a single 2D material to satisfy simultaneously the requirements for both acid and neutral conditions. Our results

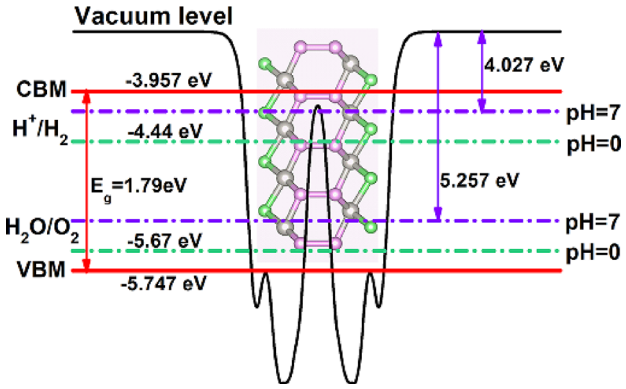

Fig. 5. Band edge alignments of the PtPS monolayer. The redox potentials are indicated by the dot-dashed lines corresponding to the values at pH = 0 and pH = 7.

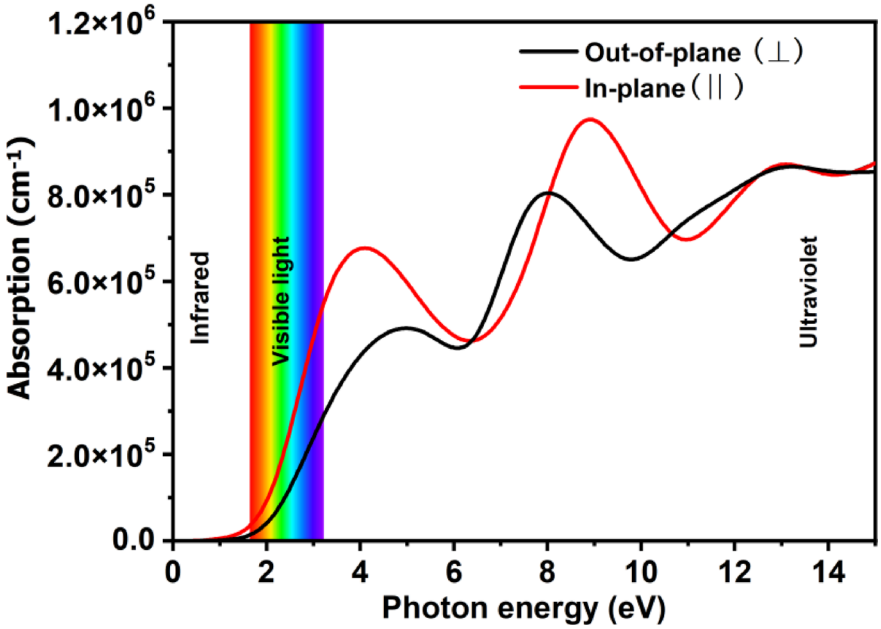

Fig. 6. The light absorption coefficient of PtPS monolayer.

indicate that the hexagonal PtPS monolayer is a promising photocatalyst for water splitting under both acidic and neutral conditions.

In addition to the requirements of the band gap and band edge position, the light harvesting performance is another important factor for an ideal photocatalyst. Figure 6 presents the absorption coefficient as a function of photon energy for in-plane (E⊥z) and out-of-plane (E ∥ z) polarization. The PtPS monolayer exhibits significant light absorption starting at approximately ~ 1.80 eV and the absorption coefficients reach values on the order of 10^5 cm^{-1}, comparable to those observed in organic perovskite solar cells[59,60]. The material demonstrates strong absorption from the visible-light to ultraviolet region, indicating its superior light-harvesting ability.

Solar-to-hydrogen efficiency

The efficiency of converting solar energy into hydrogen, commonly referred to as solar-to-hydrogen (STH) efficiency, is essential for assessing the effectiveness of technologies in photocatalytic water splitting. The STH efficiency is determined by the following formula:

$$\eta_{STH} = \eta_{\mathrm{abs}} \times \eta_{\mathrm{cu}} \tag{5}$$

where η_{abs} and η_{cu} represent the light absorption efficiency and charge carrier utilization efficiency, respectively. The η_{abs} and η_{cu} are evaluated by the following Eqs[61,62].:

$$\eta_{\mathrm{abs}} = \frac{\int_{E_g}^{\infty} P(\hbar\omega)d(\hbar\omega)}{\int_{0}^{\infty} P(\hbar\omega)d(\hbar\omega)} \tag{6}$$

$$\eta_{\mathrm{cu}} = \frac{\Delta G \int_{E}^{\infty} \frac{P(\hbar\omega)}{\hbar\omega} d(\hbar\omega)}{\int_{E_g}^{\infty} P(\hbar\omega)d(\hbar\omega)} \tag{7}$$

Here, $P(\hbar\omega)$ represents the AM 1.5G solar irradiation at the photon energy $\hbar\omega$, E_g represents the band gap of the PtPS monolayer, ΔG represents the oxidation-reduction potential difference of water (1.23 eV), E represents the energy of photons that are related to the overpotentials $\chi(H_2)$ and $\chi(O_2)$. Taking into account the energy losses associated with charge carrier migration in the material, the overpotentials for HER and OER are set at 0.2 and 0.6 eV, respectively. E can be expressed as[63]:

$$E = \begin{cases} Eg, & (\chi\ (\mathrm{H_2}) \geq\ 0.2,\ \chi\ (\mathrm{O_2}) \geq\ 0.6) \\ Eg + 0.2 - \chi\ (\mathrm{H_2})\,, & (\chi\ (H_2) < 0.2,\ \chi\ (\mathrm{O_2}) \geq\ 0.6) \\ Eg + 0.6 - \chi\ (\mathrm{O_2})\,, & (\chi\ (\mathrm{H_2}) \geq\ 0.2,\ \chi\ (\mathrm{O_2}) < 0.6) \\ Eg + 0.8 - \chi\ (\mathrm{H_2}) - \chi\ (\mathrm{O_2})\,, & (\chi\ (\mathrm{H_2}) < 0.2,\ \chi\ (O_2) < 0.6) \end{cases} \tag{8}$$

Here, $\chi(H_2)$ and $\chi(O_2)$ represent the overpotential energy of the hydrogen and oxygen evolution reactions, respectively. To realize practical large-scale applications of the photocatalysis, the STH value should surpass the threshold value of 10%[64]. The calculated value of STH for PtPS monolayer is 16.0% under acid condition, slightly smaller than the recently reported the value of P_3S (17.7%)[65], but higher than many other STH values of the materials such as GeN_3(12.63%) and Al_2Se_3(9.1%)[63,66]. The STH efficiency suggest that the PtPS monolayer can enhance the photocatalytic performance to some extent. With the pH increasing up to 7, the value ofη_{STH} is reduced to 10.47% and still remains consistently above 10%. These results suggest that the photocatalytic performance of PtPS monolayer can be significantly affected by the pH values of aqueous solution.

Hydrogen evolution reaction

The adsorption of water molecules is an essential initial step in the photocatalytic water splitting process. We calculated the adsorption energies of the water molecules at the top sites of the Pt and S atoms of PtPS monolayer. The adsorption energy can be written as:

$$E = E_{(\mathrm{PtPS+H_2O})} - E_{\mathrm{PtPS}} - E_{\mathrm{H_2O}} \tag{9}$$

where $E_{\mathrm{PtPS}} + \mathrm{H_2O}$, E_{PtPS}, and $E_{\mathrm{H_2O}}$ are the energies of the adsorbed PtPS equilibrium system, isolated PtPS monolayer, and isolated H_2O molecule, respectively. The adsorption energies for the top sites of Pt and S are −0.049 and −0.010 eV, respectively. The calculated results indicate the water molecules prefer the stably adsorbed sites on top of the Pt atom.

The Gibbs free energy is calculated to evaluate the hydrogen evolution reaction (HER) catalytic activity, which is determined by[67]

$$\Delta G = \Delta E_{\mathrm{H}} + \Delta E_{ZPE} - T\Delta S \tag{10}$$

Where ΔE_{H}, ΔE_{ZPE}, and ΔS represent the hydrogen adsorption energy, zero-point energy and entropy correction term, respectively. For the HER process in an aqueous solution, the chemical formula can be written as follows:

$$* + \mathrm{H^+} + e^- \rightarrow \mathrm{H^*} \tag{11}$$

$$\mathrm{H^*} + \mathrm{H^+} + e^- \rightarrow * + \mathrm{H_2} \tag{12}$$

Here, notation "*" is the adsorption sites on the PtPS monolayer, H* represents the intermediate state formed by H^+ adsorbed on the catalyst surface, which reacts with $(H^+ + e^-)$ in water to form H_2. This reaction step requires the photon energy absorbed by the material to be greater than the reduction potential of H^+. In Fig. 7, under conditions without illumination (U = 0), the $\Delta G_{\mathrm{H}*}$is 0.62 eV, indicating that the HER process cannot proceed spontaneously. However, when illumination is applied (U = 1.23 V), the $\Delta G_{\mathrm{H}*}$ for two steps becomes downhill, thereby enabling the reaction to proceed spontaneously. This result further suggests that the 2D hexagonal PtPS monolayer is an excellent photocatalytic material for water splitting.

Conclusion

In this research, we identified a novel stable hexagonal PtPS monolayer structure through a combination of global structure search and first-principles calculations. The structural stability, electronic transport, photocatalytic water splitting and optical absorption of the PtPS monolayer were investigated. It is found to be stable dynamically and thermally by using phonon spectra and AIMD calculations. In addition, calculated electronic properties show that the PtPS monolayer is not only an indirect semiconductor, but also exhibits anisotropic carrier mobility with electron mobility up to 5049.35 $cm^2V^{-1}s^{-1}$ along y direction. It is also revealed that the band edge positions of the PtPS monolayer meet the criteria for photocatalytic water splitting in both acidic and neutral conditions. Optical property calculations demonstrate that PtPS materials have excellent

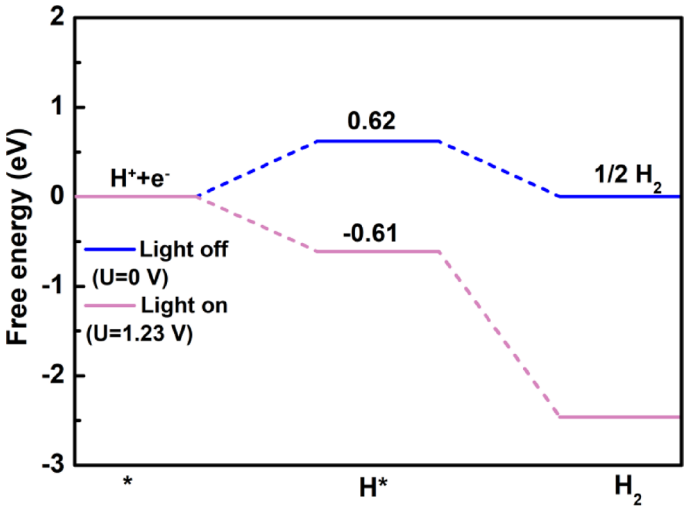

Fig. 7. The Gibbs free energy of the HER for PtPS monolayer.

light-harvesting capabilities from the visible to the ultraviolet spectral range. Furthermore, PtPS monolayer achieves a high photcatalytic water-splitting efficiency of 16.0% in acid condition. These outstanding properties suggest that the hexagonal PtPS monolayer is a promising candidate material for application in photocatalysis and nanoelectronic devices.

Data availability

The datasets used and analysed during the current study available from the corresponding author on reasonable request.

Received: 28 February 2025; Accepted: 6 May 2025
Published online: 21 May 2025

References

1. Novoselov, K. S. et al. Electric field effect in atomically thin carbon films. *science*. 306, 666–669 (2004).
2. Lin, Y. C. et al. Recent advances in 2D material theory, synthesis, properties, and applications. *ACS Nano*. **17**, 9694–9747 (2023).
3. Kim, K. S. et al. Large-scale pattern growth of graphene films for stretchable transparent electrodes. *Nature* **457**, 706–710 (2009).
4. Castro Neto, A. H., Guinea, F., Peres, N. M., Novoselov, K. S. & Geim, A. K. The electronic properties of graphene. *Rev. Mod. Phys.* **81**, 109–162 (2009).
5. Das, S., Robinson, J. A., Dubey, M., Terrones, H. & Terrones, M. Beyond graphene: progress in novel two-dimensional materials and Van der Waals solids. *Annu. Rev. Mater. Sci.* **45**, 1–27 (2015).
6. Wood, J. D. et al. Effective passivation of exfoliated black phosphorus transistors against ambient degradation. *Nano Lett.* **14**, 6964–6970 (2014).
7. Almayyali, A. O. M., Kadhim, B. B. & Jappor, H. R. Stacking impact on the optical and electronic properties of two-dimensional MoSe2/PtS2 heterostructures formed by PtS_2 and $MoSe_2$ monolayers. *Chem. Phys.* **532**, 110679 (2020).
8. Chaurasiya, R. & Dixit, A. Ultrahigh sensitivity with excellent recovery time for NH_3 and NO_2 in pristine and defect mediated Janus WSSe monolayers. *Phys. Chem. Chem. Phys.* **22**, 13903–13922 (2020).
9. Bafekry, A. et al. Embedding of atoms into the nanopore sites of the C_6N_6 and C_6N_8 porous carbon nitride monolayers with tunable electronic properties. *Phys. Chem. Chem. Phys.* **22**, 6418–6433 (2020).
10. Bafekry, A. et al. Two-dimensional carbon nitride C_6N nanosheet with egg-comb-like structure and electronic properties of a semimetal. *Nanotechnology* **32**, 215702 (2021).
11. Bafekry, A., Yagmurcukardes, M., Akgenc, B., Ghergherehchi, M. & Nguyen, C. V. Van der Waals heterostructures of MoS_2 and Janus mosse monolayers on graphitic boron-carbon-nitride (BC_3, C_3N, C_3N_4 and C_4N_3) nanosheets: a first-principles study. *J. Phys. D*. **53**, 355106 (2020).
12. Ronneberger, I., Zanolli, Z., Wuttig, M. & Mazzarello, R. Changes of structure and bonding with thickness in chalcogenide thin films. *Adv. Mater.* **32**, 2001033 (2020).
13. Tan, X. et al. Optimizing the thermoelectric performance of In–Cd codoped SnTe by introducing Sn vacancies. *J. Mater. Chem. C.* **5**, 7504–7509 (2017).
14. Oyedele, A. D. et al. $PdSe_2$: pentagonal two-dimensional layers with high air stability for electronics. *J. Am. Chem. Soc.* **139**, 14090–14097 (2017).
15. Kempt, R., Kuc, A. & Heine, T. Two-Dimensional Noble-Metal chalcogenides and phosphochalcogenides. *Angew. Chem. Int. Ed.* **59**, 9242–9254 (2020).
16. Pi, L. et al. Recent progress on 2D noble-transition-metal dichalcogenides. *Adv. Funct. Mater.* **29**, 1904932 (2019).
17. Chen, E., Xu, W., Chen, J. & Warner J. 2D layered noble metal dichalcogenides (Pt, Pd, Se, S) for electronics and energy applications. *Mater. Today Adv.* **7**, 100076 (2020).
18. Zhao, Y. et al. Low-symmetry $PdSe_2$ for high performance thermoelectric applications. *Adv. Funct. Mater.* **30**, 2004896 (2020).
19. Cheng, P. K., Tang, C. Y., Wang, X. Y., Zeng, L. H. & Tsang, Y. H. Passively Q-switched and femtosecond mode-locked erbium-doped fiber laser based on a 2D palladium disulfide (PdS_2) saturable absorber. *Photonics Res.* **8**, 511–518 (2020).
20. Lu, L. S. et al. Layer-dependent and in-plane anisotropic properties of low-temperature synthesized few-layer $PdSe_2$ single crystals. *ACS Nano*. **14**, 4963–4972 (2020).

21. Hoffman, A. N. et al. Exploring the air stability of $PdSe_2$ via electrical transport measurements and defect calculations. *Npj 2D Mater. Appl.* **3**, 50 (2019).
22. Liang, Q. et al. High-performance, room temperature, ultra-broadband photodetectors based on air-stable $PdSe_2$. *Adv. Mater.* **31**, 1807609 (2019).
23. Gu, Y. et al. Two-dimensional palladium diselenide with strong in-plane optical anisotropy and high mobility grown by chemical vapor deposition. *Adv. Mater.* **32**, 1906238 (2020).
24. Zeng, L. H. et al. Controlled synthesis of 2D palladium diselenide for sensitive photodetector applications. *Adv. Funct. Mater.* **29**, 1806878 (2019).
25. Ahmad, S. Strain and electric field dependent variation in electronic and thermoelectric properties of PtS_2. *Results Phys.* **17**, 103088 (2020).
26. Lan, Y. S., Chen, X. R., Hu, C. E., Cheng, Y. & Chen, Q. F. Penta-PdX_2 (X = S, Se, Te) monolayers: promising anisotropic thermoelectric materials. *J. Mater. Chem. A*. **7**, 11134–11142 (2019).
27. Di Bartolomeo, A. et al. Pressure-tunable ambipolar conduction and hysteresis in thin palladium diselenide field effect transistors. *Adv. Funct. Mater.* **29**, 1902483 (2019).
28. Di Bartolomeo, A. et al. Electron irradiation of multilayer $PdSe_2$ field effect transistors. *Nanotechnology* **31**, 375204 (2020).
29. Ryu, J. H. et al. Compositional effect in pentagonal layered $PdSe_{2-x}S_x$ solid-solutions and their transport properties. *Scripta Mater.* **182**, 6–10 (2020).
30. Xiao, F. et al. Pentagonal two-dimensional noble-metal dichalcogenide PdSSe for photocatalytic water splitting with pronounced optical absorption and ultrahigh anisotropic carrier mobility. *J. Mater. Chem. C.* **9**, 7753–7764 (2021).
31. Jing, Y., Ma, Y., Wang, Y., Li, Y. & Heine, T. Ultrathin layers of PdPX (X = S, Se): two dimensional semiconductors for photocatalytic water splitting. *Chemistry–A Eur. J.* **23**, 13612–13616 (2017).
32. Li, P. et al. Penta-PdPSe: a new 2D pentagonal material with highly in-plane optical, electronic, and optoelectronic anisotropy. *Adv. Mater.* **33**, 2102541 (2021).
33. Lee, B. et al. Fabrication of a Field-Effect transistor based on 2D novel ternary chalcogenide PdPS. *ACS Appl. Mater.* **15**, 42891–42899 (2023).
34. Cho, S. et al. Two-Dimensional Van der Waals material PdPSe: investigation on electrical transport. *ACS Appl. Electron. Mater.* **5**, 4409–4416 (2023).
35. Bafekry, A. et al. Two-dimensional penta-like PdPSe with a puckered pentagonal structure: a first-principles study. *Phys. Chem. Chem. Phys.* **24**, 9990–9997 (2022).
36. Huang, H., Li, W., Hu, C. & Fan, X. Promising novel thermoelectric materials: two-dimensional penta-like PtPX (X = S, Se, Te) nanosheets. *J. Mater. Chem. C.* **11**, 9449–9464 (2023).
37. Mortazavi, B., Shahrokhi, M., Zhuang, X., Rabczuk, T. & Shapeev, A. V. Mechanical, thermal transport, electronic and photocatalytic properties of penta-PdPS, -PdPSe and-PdPTe monolayers explored by first-principles calculations. *J. J. Mater. Chem. C.* **10**, 329–336 (2022).
38. Iqbal, T., Rehman, G., Khan, I., Ahmad, R. & Ahmad, I. Intriguing optical and photocatalytic properties of pentagonal penta-PtPS,-PtPSe and-PtPTe monolayers: A first-principle study. *J. Phys. Chem. Solids*. **177**, 111280 (2023).
39. Wang, Y., Lv, J., Zhu, L. & Ma, Y. Crystal structure prediction via particle-swarm optimization. *Phys. Rev. B—Condensed Matter Mater. Phys.* **82**, 094116 (2010).
40. Wang, Y., Lv, J., Zhu, L. & Ma, Y. CALYPSO: A method for crystal structure prediction. *Comput. Phys. Commun.* **183**, 2063–2070 (2012).
41. Gao, B. et al. Interface structure prediction via CALYPSO method. *Sci. Bull.* **64**, 301–309 (2019).
42. Kresse, G. & Furthmüller, J. Efficient iterative schemes for Ab initio total-energy calculations using a plane-wave basis set. *Phys. Rev. B*. **54**, 11169 (1996).
43. Blöchl, P. E. Projector augmented-wave method. *Phys. Rev. B*. **50**, 17953 (1994).
44. Kresse, G. & Joubert, D. From ultrasoft pseudopotentials to the projector augmented-wave method. *Phys. Rev. B*. **59**, 1758 (1999).
45. Perdew, J. P., Burke, K. & Ernzerhof, M. Generalized gradient approximation made simple. *Phys. Rev. Lett.* **77**, 3865 (1996).
46. Heyd, J., Scuseria, G. E. & Ernzerhof, M. Hybrid functionals based on a screened coulomb potential. *J. Chem. Phys.* **118**, 8207–8215 (2003).
47. Krukau, A. V., Vydrov, O. A., Izmaylov, A. F. & Scuseria, G. E. Influence of the exchange screening parameter on the performance of screened hybrid functionals. *J. Chem. Phys.* **125**, (2006).
48. Togo, A. & Tanaka, I. First principles phonon calculations in materials science. *Scripta Mater.* **108**, 1–5 (2015).
49. Bardeen, J. & Shockley, W. Deformation potentials and mobilities in non-polar crystals. *Phys. Rev. B*. **80**, 72 (1950).
50. Lin, M. et al. Two-dimensional nanoporous metal chalcogenophosphates MP_2X_6 with high electron mobilities. *Appl. Surf. Sci.* **493**, 1334–1339 (2019).
51. Dabsamut, K., Chatratin, I., Thanasarnsurapong, T., Maluangnont, T. & Boonchun, A. Theoretically proposed stable polymorph of two-dimensional pentagonal β-PdPSe. *Phys. Chem. Chem. Phys.* **25**, 3815–3819 (2023).
52. Dabsamut, K. et al. Two-Dimensional Penta-NiPS sheets: two stable polymorphs. *J. Phys. Chem. C.* **126**, 19455–19461 (2022).
53. Mouhat, F. & Coudert, F. X. Necessary and sufficient elastic stability conditions in various crystal systems. *Phys. Rev. B*. **90**, 224104 (2014).
54. Cooper, R. C. et al. Nonlinear elastic behavior of two-dimensional molybdenum disulfide. *Phys. Rev. B—Condensed Matter Mater. Phys.* **87**, 035423 (2013).
55. Wang, B. J. et al. Electronic structures and enhanced photocatalytic properties of blue Phosphorene/BSe Van der Waals heterostructures. *J. Mater. Chem. A*. **6**, 8923–8929 (2018).
56. Chen, S. & Wang, L. W. Thermodynamic oxidation and reduction potentials of photocatalytic semiconductors in aqueous solution. *Chem. Mater.* **24**, 3659–3666 (2012).
57. Shahid, I. et al. Two dimensional MoSSe/BSe VdW heterostructures as potential photocatalysts for water splitting with high carrier mobilities. *Int. J. Hydrog. Energy*. **46**, 14247–14258 (2021).
58. Hu, W., Lin, L., Zhang, R., Yang, C. & Yang, J. Highly efficient photocatalytic water splitting over edge-modified phosphorene nanoribbons. *J. Am. Chem. Soc.* **139**, 15429–15436 (2017).
59. Jeon, N. J. et al. Solvent engineering for high-performance inorganic–organic hybrid perovskite solar cells. *Nat. Mater.* **13**, 897–903 (2014).
60. Shirayama, M. et al. Optical transitions in hybrid perovskite solar cells: ellipsometry, density functional theory, and quantum efficiency analyses for $CH_3NH_3PbI_3$. *Phys. Rev. Appl.* **5**, 014012 (2016).
61. Chen, Z. et al. Accelerating materials development for photoelectrochemical hydrogen production: standards for methods, definitions, and reporting protocols. *J. Mater. Res.* **25**, 3–16 (2010).
62. Zhan, L. B., Yang, C. L., Wang, M. S. & Ma, X. G. Discovery of two-dimensional Ga_2S_3 monolayers for efficient photocatalytic overall water splitting to produce hydrogen. *Appl. Surf. Sci.* **626**, 157215 (2023).
63. Fu, C. F. et al. Intrinsic electric fields in two-dimensional materials boost the solar-to-hydrogen efficiency for photocatalytic water splitting. *Nano Lett.* **18**, 6312–6317 (2018).
64. Fox, M. *Optical Properties of Solids* (Oxford University Press, 2010).
65. Shao, L. et al. Theoretical study on binary monolayer P3S-I for photocatalytic overall water plitting. *Chemistry–A Eur. J.* **31**, e202404312 (2025).

66. Liu, J. et al. GeN_3 monolayer: A promising 2D high-efficiency photo-hydrolytic catalyst with high carrier mobility transport anisotropy. *Appl. Catal. B.* **279**, 119368 (2020).
67. Zhang, W., Xi, S., Liang, Y. & He, C. Construction of novel PG/GeP_2 and PG/SiP_2 VdW heterostructures for high-efficiency photocatalytic water splitting. *Appl. Surf. Sci.* **608**, 155106 (2023).

Author contributions
C. Pu and D. Zhou wrote the main manuscript text, review and editing. P. Zhang and L. Chen conducted a detailed formal analysis of the manuscript. All authors reviewed the manuscript. C.Pu and X. Pan mainly responsible for the methodology and calculations. D. Zhou provided the software.

Funding
This research was supported by the National Natural Science Foundation of China (Nos. U1904612, 12405312).

Declarations

Competing interests
The authors declare no competing interests.

Conflict of interest
There are no conflicts to declare.

Additional information
Correspondence and requests for materials should be addressed to D.Z.

Reprints and permissions information is available at www.nature.com/reprints.

Publisher's note Springer Nature remains neutral with regard to jurisdictional claims in published maps and institutional affiliations.